BBA - Molecular Basis of Disease 1865 (2019) 587–598

Contents lists available at ScienceDirect

BBA - Molecular Basis of Disease

journal homepage: www.elsevier.com/locate/bbadis

SIRT1 activation by SRT1720 attenuates bone cancer pain via preventing Drp1-mediated mitochondrial fission

Ming-Yue Li[b,1], Jie-Qiong Ding[a,1], Qiong Tang[a,1], Miao-Miao Hao[b], Bang-Hua Wang[a], Ji Wu[a], Liang-Zhu Yu[a], Ming Jiao[a], Bin-Hua Luo[b], Min Xie[a,*], Hai-Li Zhu[a,*]

[a] Research Center of Basic Medical Sciences, Department of Physiology, School of Basic Medical Sciences, Hubei University of Science and Technology, Xianning 437100, China

[b] School of Pharmacy, Hubei University of Science and Technology, Xianning 437100, China

ARTICLE INFO

Keywords:
Bone cancer pain
Spinal cord
Silent information regulator 1 (SIRT1)
Dynamin-related protein 1 (Drp1)
SRT1720

ABSTRACT

Bone cancer pain (BCP) is the pain induced by primary bone cancer or tumor metastasis. Increasing evidence and our previous studies have shown that mammalian silent information regulator 2 homolog (SIRT1) is involved in periphery sensitization and central sensitization of BCP, and the underlying mechanism of SIRT1 in bone cancer pain may provide clues for pain treatment. Dynamin-related protein 1 (Drp1) is an essential regulator for mitochondrial fission. In this research, BCP model rats were established by injecting MRMT-1 rat mammary gland carcinoma cells into the left tibia of female Sprague-Dawley rats and validated by tibia radiographs, histological examination and mechanical pain test. As a result BCP rats exhibited bone destruction and sensitivity mechanical pain. BCP increased inflammatory cells infiltration and apoptosis, reduced SIRT1 protein expression and phosphorylation, and elevated Drp1 expression in spinal cord. An agonist of SIRT1 named SRT1720 intrathecal treatment in BCP rats increased SIRT1 phosphorylation, reduced the up-regulated Drp1 expression, and reversed pain behavior. SRT1720 also regulated Bcl-2/BAX and cleaved caspase-3 expressions, and inhibited mitochondrial apoptosis in spinal cord of BCP rats. For in vitro research, SRT1720 treatment decreased Drp1 expression in a dose-dependent manner, blocked CCCP-induced mitochondrial membrane potential change, consequently reduced apoptosis and promoted proliferation. These data suggest that SIRT1 activation by SRT1720 attenuated bone cancer pain via preventing Drp1-mediated mitochondrial fission. Our results provide new targets for therapeutics of bone cancer pain.

1. Introduction

Bone cancer pain (BCP) is the pain induced by primary bone cancer or tumor metastasis [1]. Bone metastasis arises more commonly in patients with breast, prostate, kidney and lung cancers. When tumor cells begin to grow in bone, tumor growth causes bone destruction, woven bone formation, and a significant bone pain [2]. BCP is usually described as dull in character, constant in presentation, and gradually intensifies to severe incident pain, which debilitates the quality of patients' life and their functional status [3]. Pathology of BCP is complex and unique, mixing with inflammatory, neuropathic pain and tumor-specific mechanisms [4]. Despite a variety of factors are linked to bone cancer pain, the specific cellular and molecular mechanisms underlie the pathogenesis of bone cancer pain remain unclear, and the effective clinical approaches are needed for its treatment. To date the therapeutic avenue for BCP are pharmacotherapy and chemotherapeutics. The mainstay symptomatic treatment for bone cancer pain is opioid-based pharmacotherapy, but the limited effectiveness and side-effects prohibit the widespread use of the drugs [5,6]. Non-steroidal anti-inflammatory drugs treatment is helpful, but with gastrointestinal, cardiovascular and renal risk [7]. Consequently, further research is needed to develop more effective strategies and treatment based on the different mechanisms of BCP.

Mammalian silent information regulator 2 homolog (SIRT1) is a nicotinamide adenosine dinucleotide (NAD)-dependent deacetylase that removes acetyl groups from proteins, and functions in oxidative stress, apoptosis and autophagy [8]. It is reported that SIRT1 plays critical roles in various types of pain, including inflammatory pain [9,10], neuropathic pain [11,12] and bone cancer pain [13]. In rodent models of inflammatory pain and neuropathic pain, both the expression

* Corresponding authors.
E-mail addresses: mmtmrxm@sina.com, hkhaili_zhu@163.com (H.-L. Zhu).
[1] Contributed equally to this work.

https://doi.org/10.1016/j.bbadis.2018.12.017
Received 30 August 2018; Received in revised form 29 November 2018; Accepted 18 December 2018
Available online 20 December 2018

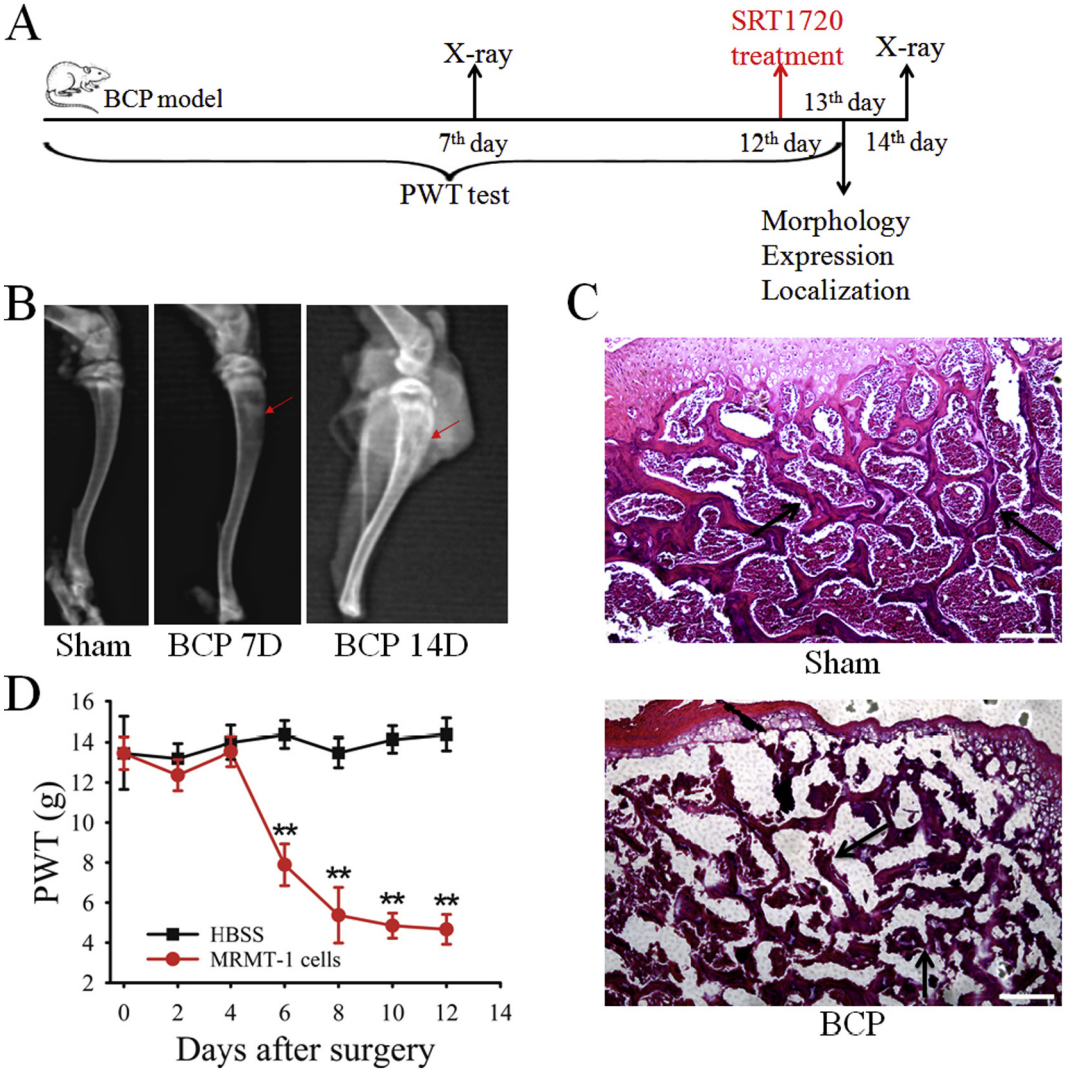

Fig. 1. Intra-tibia MRMT-1 cell injection induced bone destruction and mechanical allodynia in BCP rats. A. Experimental protocol showed establishment of BCP model, behavioral and morphological tests on certain day. B. After injection of MRMT-1 cells (3×10^5) into the intramedullary space of left tibia on BCP rats. X-ray examination indicated the degree of bone destruction in sham rats and BCP rats on 7 (second lane) and 14 (third lane) day after surgery. C. H&E straining of bone slices showed changes of bone trabeculae in sham and BCP rats. Arrows in sham group pointed out continuous thick bone trabeculae, and arrows in BCP group pointed out discontinuous bone trabeculae. Scale bar = 200 μm. D. Mechanical PWT showed that BCP rats were mechanical allodynia. PWT was tested using a series of calibrated von Frey filaments prior to tumor cell inoculation (0 day) and at post-operative day (POD) 2, 4, 6, 8, 10 and 12 (black □: sham group, red ●: model group). All data were expressed as the mean ± SEM, n = 9. $^{**}P < 0.01$ vs. the HBSS group rats at each corresponding time point.

and activity of SIRT1 are down-regulated in neurons of dorsal root ganglion (DRG) [13] and spinal cord [11]. In addition, chemical agents acting on SIRT1 activity have obvious effect on augmentation or alleviation of pain. SIRT1 agonist treatment alleviates spontaneous pain, thermal hyperalgesia, and mechanical allodynia [13,14], while SIRT1 inhibitor aggravates the nociceptive effect [12]. Induction of pain is depended on activation of certain ion channels in pathways of pain perception. Metabotropic glutamate receptor (mGluR1) and mGluR5 plays essential roles in nociceptive processing via increasing the opening of cation channels (such as Ca^{2+}, Na^+ and K^+ channels). SIRT1 is involved in the regulation of mGluR1/5 expression [15]. Through regulating these receptors, SIRT1 is implicated in central sensitization of pain. In addition, SIRT1 was involved in periphery sensitization by regulating the expression of acid-sensing ion channels 3 (ASIC3) in DRG neuron [13]. Accordingly, SIRT1 is a critical regulator of BCP and could be a potential therapeutic target for bone cancer pain.

Neurons are metabolically active cells with high energy demands and particularly dependent on mitochondrial function [16]. As a dynamic organelle, mitochondrion is known for its critical roles in energy metabolism, cell survival, and synaptic plasticity [17]. Mitochondrial fission maintains mitochondrial structure, and alterations in fission process are linked to many human diseases, such as neurodegenerative disease [18,19], cancers [20] and metabolic disorders [21]. Dynamin-related protein 1 (Drp1), a cytosolic GTPase, migrates between the cytosol and the mitochondrial network, binds to mitochondrial outer membrane, and drives mitochondrial fission [18]. *Drp1* homozygous knockout mice are lethal in embryos due to reduced mitochondrial fission [22]. *Drp1* gene mutations lead to abnormal brain development, optic atrophy and neonatal lethality [23]. Dysregulation of Drp1 is related to mitochondrial dysfunction-mediated pain. In the perineural HIV coat glycoprotein gp120-induced neuropathic pain rats, increase of Drp1 expression in spinal cord is observed while antisense oligodeoxynucleotide against Drp1 treatment attenuated mechanical allodynia [24,25].

In order to evaluate the effect of SIRT1 on Drp1 expression and mitochondrial fission in bone cancer pain, we used SRT1720 (N-[2-[3-(piperazin-1-ylmethyl) imidazo [2,1-b] [1,3] thiazol-6-yl] phenyl] quinoxaline-2-carboxamide), a specific agonist of SIRT1 [26], to

activate SIRT1 and detect Drp1 expression and mitochondrial-mediated apoptosis in BCP rats. Our data demonstrated that SIRT1 activation attenuated bone cancer pain via reversing Drp1-mediated mitochondrial fission.

2. Materials and methods

2.1. Animals and SRT1720 treatment

Animals used for bone cancer pain model and all experiments were female Sprague-Dawley (SD) rats weighing 160–200 g (6–8 weeks) and purchased from Hubei Province Experimental Animal Center (Wuhan, CHN). The experimental procedures were confirmed to the local and international guidelines on ethical use of animals, and all efforts were made to minimize the number of animals used and their sufferings.

For intrathecal injection, rats were held firmly, and 25 μl microsyringe was inserted between L5 and L6 vertebrae. A sudden advancement of the needle accompanied by a slight flick of the tail was used as the indicator for the proper insertion into the subarachnoid space [27]. SRT1720 (10 μl) was injected slowly, and the concentration for rats was 0.5 mg/kg [28]. SRT1720 (Sigma-Aldrich) was dissolved in dimethyl sulfoxide (DMSO) (Sigma-Aldrich) to prepare the stock solution, and diluted by 0.9% NaCl (v/v = 1:1) before use. Vehicle was injected with same volume (10 μl) of DMSO and 0.9% NaCl. For cell experiments, SRT1720 was diluted with DMSO to different concentrations.

2.2. Experimental protocol

Rats were randomly divided into three experimental groups: sham group rats treated with vehicle (Sham), BCP group rats treated with vehicle (BCP), BCP group rats treated with SRT1720 (BCP + SRT1720), each group contains 9–12 animals. The process was described in Fig. 1A. Surgery operation day was day 0. The 50% paw withdrawal threshold (PWT) of rats was tested at post-operative day (POD) 0, 2, 4, 6, 8, 10 and 12. X-ray of rats was tested at POD 7 and 14. SRT1720 and vehicle treatment on rats were at POD 12. After treated 12 h, morphology, expressions and localizations were tested.

2.3. Preparation of cells

MRMT-1 rat mammary gland carcinoma cells were purchased from JENNIO Biological Techonology (Guangdong, CHN). Cells were cultured in medium containing RPMI 1640 (GIBCO), supplemented with 10% fetal bovine serum (FBS) (GIBCO), 1% L-glutamine and 2% penicillin/streptomycin (GIBCO). Cells were digested with 0.25% trypsin (GIBCO), washed twice with PBS (135 mM NaCl, 4.7 mM KCl, 10 mM Na_2HPO_4, 2 mM NaH_2PO_4, pH 7.4), and suspended in HBSS (Hanks' Balanced Salt Solution, 137.93 mM NaCl, 5.33 mM KCl, 4.17 mM $NaHCO_3$, 0.441 mM KH_2PO_4, 0.338 mM Na_2HPO_4, 5.56 mM D-Glucose) at a concentration of 3×10^7 cells/ml. HBSS was also used for inoculation in sham rats.

2.4. Rat model of BCP

In order to imitate bone metastasis of breast cancer, MRMT-1 rat mammary gland carcinoma cells were used to establish bone cancer pain model. Female SD rats were used due to higher breast cancer incidence and mortality in female than male [29]. BCP rat model was established following previous reports [6]. In brief, female SD rats were deeply anesthetized with pentobarbital sodium (50 mg/kg, intraperitoneal injection). Left leg of rat was shaved and the top half of the tibia was carefully exposed after disinfection with 7% iodine and 75% (v/v) ethanol. 3×10^5 MRMT-1 cells were slowly injected into the intramedullary space of BCP rats' left tibia, whereas an equivalent volume of HBSS was injected into the same position of sham rats using a 50 μl Hamilton microsyringe. Syringe was left in the injection site for an additional minute to prevent the leakage of tumor cells. Injection site was sealed with bone wax after syringe was removed. To evaluate tumor growth, tibia was visualized radiographically.

2.5. Mechanical allodynia

The 50% paw withdrawal threshold (PWT) to a static mechanical stimulus was assessed using von Frey filaments and Chaplan's up-and-down method [30]. Rats were placed on a 5 × 5-mm wire mesh grid floor and allowed to habituate for 30 min. Tests were blind with respect to group. The von Frey filaments (Stoelting) (ranging from 0.4 g to 26 g) were used to apply mechanical stimuli to the left hind paw. In brief, the calibrated monofilaments were applied perpendicularly to the plantar surfaces until the filaments were bent, and a brisk withdrawal was considered as positive response. Whenever a positive response occurred, the von Frey filament of the next lower force was applied, and whenever a negative response occurred, the filament of the next higher force was applied. Then, the pattern of positive and negative withdrawal responses was converted to 50% PWT.

2.6. RNA extraction and quantitative real-time PCR

On day 12–14 following inoculation of MRMT-1 cells or HBSS, rats were sacrificed and their spinal cords were removed. Ipsilateral spinal cord was washed with ice-cold PBS, incubated with TRIzol reagent (Invitrogen) in RNase free tubes, and mixed with chloroform (200 μl/ml TRIzol). After centrifugation for 10 min at 13,525 g, an equal volume of isopropanol was added to the supernatant and centrifuged at 13,525 *g* for 10 min. After removing the supernatant, 75% ethanol was added, and the mixture centrifuged at 13,525 *g* for 10 min. The resulting pellet was dissolved with RNase free water. RNA concentrations were adjusted based on absorbance at 260 nm. After reverse transcription, analysis of *Drp1* gene expression was performed by qRT-PCR on Light Cycler 96 instrument (Roche Diagnositics Ltd) with SYBR Green Master Mix (Vazyme). Real-time PCR was performed in 20 μl reaction volumes containing SYBR Green Master Mix (10 μl), cDNA templates (100 ng), primers (2 μl) and RNase free water. The original mRNA copies were evaluated by $2^{-\Delta\Delta CT}$ method, and relative *Drp1* mRNA concentrations were normalized to GADPH. *Drp1* forward and reverse primer sequences were 5'-ACAACAGGAGAAGAAAATGGAGT-3′ and 5'-GATGGATTGGCTCAGGGCTT-3′. GAPDH was used as the internal control, forward and reverse primer sequences were 5'-AACTTTGGCATCGTGGAA-3′ and 5'-TACATTGGGGGTAGGAACAC-3′.

2.7. Western blot

Ipsilateral spinal cord was collected and homogenized in a RIPA lysis buffer (50 mM Tris, 150 mM NaCl, 1% Triton X-100, 1% sodium deoxycholate,0.1% SDS, sodium orthovanadate, sodium fluoride, EDTA, leupeptin, pH 7.4) containing a cocktail of protease inhibitors (200 mM AEBSF, 30 μM aprotinin, 13 mM bestatin, 1.4 mM E64 and 1 mM leupeptin, 100 mM EDTA, 100×, Sigma-Aldrich). After centrifugation at 13,525 *g* for 15 min, supernatant was used for western blotting analysis. Equal amounts of protein samples were separated in 10% SDS-polyacrylamide gel electrophoresis. The protein was transferred onto a PVDF membrane, blocked with 5% defatted milk in TBST (10 mM Tris-HCl, 150 mM NaCl, 0.1% (v/v) Tween-20, pH 7.5), then incubated with the appropriate primary antibodies including mouse anti-SIRT1 (1:1000, A0127, ABclonal Technology), rabbit anti-pSer47-SIRT1 (1:1000, PA5–17391, Thermo Fisher), rabbit anti-Drp1(1:1000, A2586, ABclonal Technology), rabbit anti-pSer637-Drp1 (1:1000, AP0812, ABclonal Technology), rabbit anti-PGC-1α (1:1000, A12348, ABclonal Technology), anti-Bcl-2 (1:500, MA1–26233, Thermo Fisher), rabbit anti-caspase-3 (1:1000, A11319, ABclonal Technology,), anti-β-actin (1:5000, A1978, Sigma-Alchdrich) overnight. HRP-conjugated

secondary antibodies (1:5000, ABclonal Technology) were used to visualize the primary antibodies. Infrared Imaging System (Gene Company Limited) was applied to detect immunoreactive bands.

2.8. Haematoxylin and eosin (H&E) staining

On day 14 following inoculation of MRMT-1 cells or HBSS, rats deeply anesthetized with pentobarbital sodium (50 mg/kg, intraperitoneal injection), perfused with PBS followed by 4% paraformaldehyde. Left tibial tissue was removed, preserved in 10% neutral buffered formalin, decalcified using 10% EDTA for 21 days, embedded in paraffin, sectioned to 5-μm-thick (Leica RM 2165), and stained using standard Haematoxylin and Eosin (H&E) method. Spinal cord was dissected out, post fixed for 12 h, and incubated in 20% (w/v) sucrose in PBS for 24 h at 4 °C, followed by freezing in isopentane (−40 °C). 8 μm coronal sections cut on freezing microtome/cryostat for standard H&E staining.

2.9. Immunofluorescene

Rats were anesthetized, perfused with PBS followed by 4% paraformaldehyde. Spinal cord were dissected out, post fixed for 12 h, prepared for paraffin embedding, cut into 5 μm sections and stained with antibodies. For cells, cells were seeded onto glass slides for different treatment. Then, cells were washed, fixed with 4% paraformaldehyde, permeabilized with Triton X-100, blocked with 10% goat serum and stained with antibodies. Primary antibodies: mouse anti-NeuN (1:100, ab104225, Abcam), mouse anti-SIRT1 (1:100, A0127, ABclonal Technology), rabbit anti-PGC-1α (1:1000, A12348, ABclonal Technology), anti-Bcl-2 (1:500, MA1–26233, Thermo Fisher), rabbit anti-activated-caspase-3 (1:1000, A11021, ABclonal Technology), rabbit anti-pSer637-Drp1 (1:1000, AP0812, ABclonal Technology) and rabbit anti-Drp1(1:100, A2586, ABclonal Technology). Secondary antibodies: goat anti-rabbit or mouse IgG H&L (FITC and TRITC) (Abcam).

2.10. ELISA kit

Ipsilateral spinal cord was homogenized and homogenized using PBS buffer pH 7.4 containing a protease inhibitor cocktail. BAX levels in spinal cord lysates were quantified by enzyme-linked immunosorbent assay (ELISA) kits from BD Biosciences. Assay was performed according to instructions provided by the manufacturer.

2.11. TUNEL assay for apoptosis

Apoptosis was detected using terminal deoxynucleotidyl transferase (TdT)-mediated dUTP-digoxigenin nick-end labeling (TUNEL) assays with a commercial TUNEL apoptosis assay kit (Beyotime). Spinal cord was dissected out, post fixed for 12 h, and incubated in 20% (w/v) sucrose in PBS for 24 h at 4 °C, followed by freezing in isopentane (−40 °C). 8 μm coronal sections cut on freezing microtome/cryostat for TUNEL assay. TUNEL assays were then performed according to the manufacturer's instructions.

2.12. EdU assay for cell proliferation

Cell proliferation was evaluated using (5-ethynyl-2′-deoxyuridine) EdU-488 assay kit (Beyotime). EdU assay protocol was performed according to the manufacturer's protocol. Cells were plated in 24-well plates. 10 μM EdU was added to wells, and plates were incubated at 37 °C for 2 h. Then, cells were washed, fixed, permeabilized and evaluated by a microscope (Olympus). Ratio of EdU-positive cells (green fluorescence) to hoechst-stained cells (with blue fluorescence) was used to evaluate cell proliferation activity. All conditions were tested in three replicates.

2.13. Isolation of cell mitochondria

Cell mitochondria were isolated using cell mitochondria isolation kit (Beyotime). Briefly, cells were digested with trypsin, washed and suspended in ice PBS, and homogenized 15–20 times. Crude mitochondrial fraction was resuspended and centrifuged at 1,000 *g* for 10 min followed by final pelleting at 11,000 g for 15 min. Isolated mitochondria were resuspended in RIPA lysis buffer containing a cocktail of protease inhibitors, and prepared for western blotting.

2.14. Statistical analysis

Comparison of values between different experimental groups was done using one-way analysis of variance (one-way ANOVA) with repeated measures followed by Bonferroni post hoc tests. Significance was ascribed for $P < 0.05$. All raw data were presented as mean ± SD, except data of PWT test was showed as mean ± SEM.

3. Results

3.1. Osteopenia and pain-related behavior are induced by carcinoma cell inoculation

MRMT-1 rat mammary gland carcinoma cells were injected into left tibia of female SD rats to establish animal model of bone cancer pain (BCP). After establishment of BCP model, behavioral and morphological tests were used to evaluate the changes in animals, and experiment procedure was shown in Fig. 1A. Parameters for bone morphology and hyperalgesia were used to detect pain induced by bone cancer. Bone density was confirmed by X-ray at 7 and 14 day after MRMT-1 cells injection into tibia. X-ray films showed on post-operative day (POD) 7 regional bone destruction was observed and on POD 14 infiltrated osteolytic lesions and bone cortex damage were found in the injection area (Fig. 1B). Histological examination further proved significant bone destruction in BCP rats (Fig. 1C). Bone slices stained with H&E showed continuous thick trabeculae in sham group and discontinuous bone trabeculae in BCP. PWT test was used to analyze the mechanical hyperalgesia. Mechanical pain sensitivity was elicited by bone cancer in BCP rats (Fig. 1D), allodynia was beginning at POD 6 (sham vs. BCP: 14.4 ± 0.7 vs. 7.9 ± 1.0; $P < 0.01$), gradually increasing at POD 8 (sham vs. BCP: 13.5 ± 0.7 vs. 5.4 ± 1.4; $P < 0.01$), and continuing to POD 12 (last time point examined; sham vs. BCP: 14.4 ± 0.8 vs. 4.7 ± 0.7; $P < 0.01$). Nevertheless, no significant changes were detected in sham rats.

3.2. SRT1720 treatment reduces BCP-induced apoptotic signal in spinal cord

Spinal dorsal horn was critical for processing sensory information, including pain perception [31]. Therefore we detected the changes in spinal dorsal horn induced by bone cancer. Histological examination showed that increased infiltration of inflammatory cells was observed in spinal dorsal horn of BCP group, compared with sham group (Fig. 2A). This result indicated progressive destruction of spinal cord was induced by bone cancer pain. TUNEL assay was designed to detect apoptotic cells that undergo extensive DNA degradation during the late stages of apoptosis [32]. Herein, we used TUNEL assay to detect the apoptotic signal in spinal cord, especially dorsal horn. Spinal dorsal horn of sham rats showed little TUNEL-positive cells, and TUNEL signal in spinal dorsal horn of BCP rats was increased significantly (Fig. 2B). Meanwhile, compared with sham rats, BCP rats showed dysregulation of apoptosis-related factors. BCP decreased anti-apoptotic factor Bcl-2 expression, increased proapoptotic factor BAX expression and apoptotic mediator cleaved caspase-3 expression level in spinal cord (Fig. 2C–E). These results suggested that apoptosis in spinal cord of BCP rats was activated.

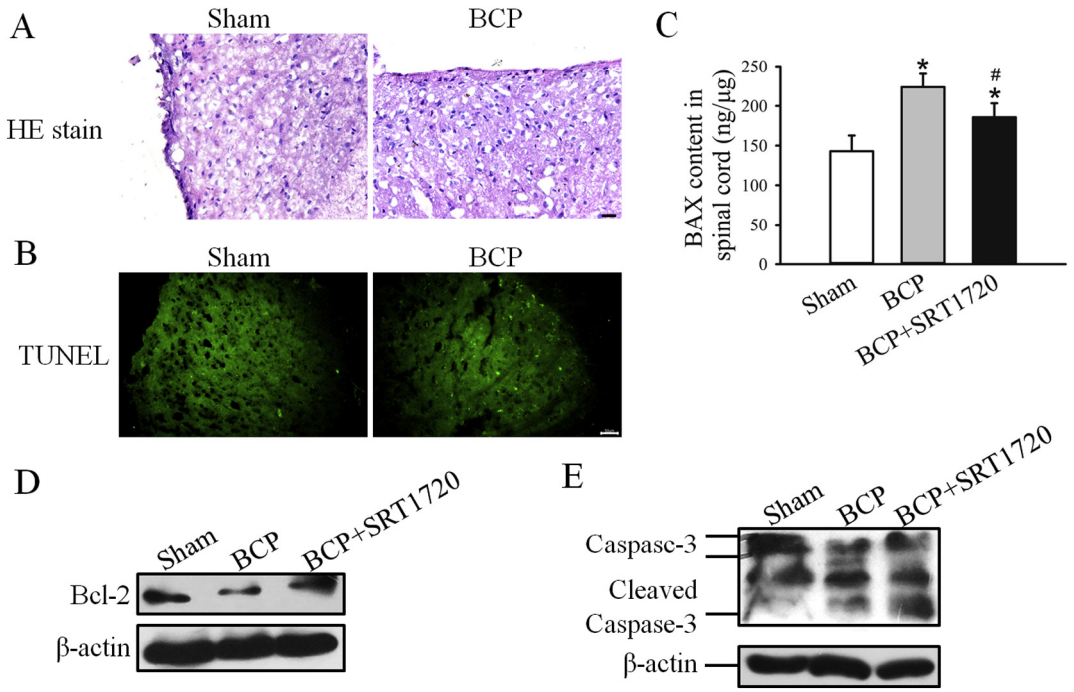

Fig. 2. Effects of SRT1720 on apoptotic signal of spinal cord. A. Representative HE staining of spinal cord showed inflammatory cell infiltration in sham and BCP rats. B. TUNEL assay detected apoptotic cells of spinal dorsal cord in sham rats and BCP rats. Scale bar = 100 μm. *C. ELISA* analysis of BAX protein content in spinal cord of sham, BCP and BCP + SRT1720 rats. $^{*}P < 0.05$ vs. sham group, $^{\#}P < 0.05$ vs. BCP group. (D-E) Western blotting analysis of Bcl-2 (D) and caspase-3 (E) protein in spinal cord of sham, BCP and BCP + SRT1720 rats.

SRT1720, a selective SIRT1 agonist, was intrathecally injected into spinal cord of BCP rats. After 12 h treatment, expression of Bcl-2, BAX and caspase-3 were detected. Results showed that SRT1720 treatment up-regulated Bcl-2 expression, and down-regulated BAX and cleaved caspase-3 expression in spinal cord of BCP rats. These data illustrated that SRT1720 inhibited apoptotic signal in spinal cord of BCP rats.

3.3. SRT1720 reverses the inhibitory effect of BCP on SIRT1 activity

To determine the role of SIRT1 in BCP, western blot was carried out to analyze SIRT1 expression and activity in spinal cord of sham rats, BCP rats and BCP + SRT1720 rats (Fig. 3). SIRT1 activity is represented by the level of phosphorylation of SIRT1 at Ser47 which is activator site and increased SIRT1 target genes expression [33]. As shown in Fig. 3, total level and phosphorylated SIRT1 were decreased in BCP group, and SRT1720 treatment recovered phosphorylation of SIRT1. Relative value of pSIRT1/SIRT1 in BCP + SRT1720 rats was 1.38 ± 0.06 ($P < 0.05$ vs. BCP group, Fig. 3D), which represented the increase in SIRT1 activity. These results suggested that SIRT1 expression and activity were decreased in BCP and SRT1720 had activator effect on SIRT1 activity.

3.4. SIRT1 activation reduces pain behavior in BCP rats

In accordance with the changes of SIRT1 activity, mechanical allodynia in BCP + SRT1720 rats was significantly ameliorated. As shown in Fig. 4A, BCP + SRT1720 rats showed a significant increase in PWT at post injection 1 h (vehicle vs. SRT1720: 5.6 ± 1.3 vs. 13.4 ± 1.0, $P < 0.05$), 3 h (vehicle vs. SRT1720: 6.3 ± 1.3 vs. 12.3 ± 1.7, $P < 0.05$), 5 h (vehicle vs. SRT1720: 5.9 ± 1.3 vs. 16.0 ± 0.8, $P < 0.05$),7 h (vehicle vs. SRT1720: 5.8 ± 1.1 vs. 12.9 ± 2.4, $P < 0.05$), 12 h (vehicle vs. SRT1720: 5.5 ± 1.2 vs. 13.2 ± 1.5, $P < 0.05$) and 18 h (vehicle vs. SRT1720: 5.3 ± 1.3 vs. 10.3 ± 1.8, $P < 0.05$). There was no significant change after SRT1720 treatment 24 h (vehicle vs. SRT1720: 5.6 ± 0.9 vs. 8.8 ± 2.1, $P > 0.05$). SRT1720 had little effect on PWT of normal rats (Fig. 4B). Taken together, SRT1720 treatment reversed pain behavior in BCP rats.

3.5. SIRT1 activation decreases Drp1-positive neurons in spinal cord of BCP rats

Drp1 is a critical protein for mitochondrial fission and is important for mitochondrial function in synaptic plasticity and neuron function [21]. Herein, to investigate the relationship between Drp1 and BCP, Drp1 expression in spinal cord was identified using double immunofluorescence staining with neuron specific marker NeuN and antibody against Drp1. Results showed that in sham rats, Drp1 (green) colocalized with NeuN (red) in the spinal dorsal horn, the percentage of Drp1/NeuN double positive neurons was 47.9 ± 3.2%. In BCP rats, the percentage of Drp1/NeuN double positive neurons was 60.8 ± 2.6%, which means more Drp1 positive neurons than that in sham rats ($P < 0.05$). Moreover, the percentage of Drp1/NeuN double positive neurons in spinal cord of BCP + SRT1720 rats was 54.8 ± 2.6%, less than BCP rats (Fig. 5), which suggested Drp1-positive neurons was reduced by SRT1720 treatment ($P < 0.05$ vs. BCP rats).

3.6. SRT1720 down-regulates Drp1 expression in spinal cord of BCP rats

Furthermore, qRT-PCR and WB were used to evaluate Drp1 expression in BCP. Data showed that Drp1 mRNA and protein expression were up-regulated in BCP rats. Relative Drp1 mRNA levels in spinal cord of BCP rats were 2.18 ± 0.08 ($P < 0.05$ vs. sham group, Fig. 6A). Treatment of SRT1720 significantly decreased Drp1 mRNA (1.28 ± 0.08, $P < 0.05$ vs. BCP rats). For protein, SRT1720 had the common effect to recover Drp1 protein level to sham level. After normalized to sham group, relative levels of Drp1 protein in BCP and BCP + SRT1720 rats were 1.34 ± 0.05 and 0.97 ± 0.05, respectively (Fig. 6B and C). To evaluate Drp1 GTPase activity in BCP rats, phosphorylation of Drp1 at Ser637 site was tested, which is an inhibited site of Drp1 GTPase activity [34,35]. Data shown that pSer637-Drp1 expression was significantly down-regulated in spinal cord of BCP rats

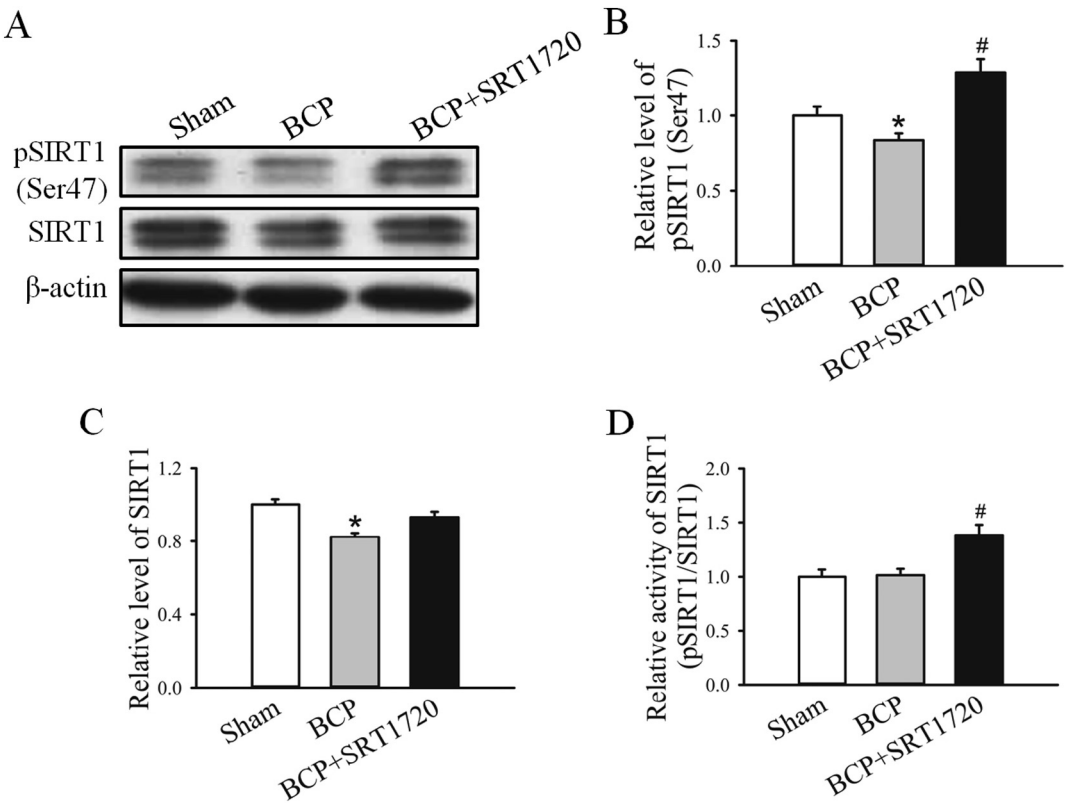

Fig. 3. Effects of SRT1720 on SIRT1 expression and phosphorylation in spinal cord of BCP rats. A. Western blot measured SIRT1 and pSIRT1 protein level. Representative blots of proteins extracted from spinal cord of sham, BCP and BCP + SRT1720 rats. B-D. Image J software were used to quantify the gray degree values. Data in B and C was normalized to the level of β-actin; Data in D was normalized to the level of total SIRT1. The density analysis was shown as mean ± SD for three independent trials. $^{*}P < 0.05$ compared with sham group. $^{\#}P < 0.05$ compared with BCP group.

($P < 0.05$ vs. sham group, Fig. 6B, D and E), presenting increased Drp1 GTPase activity. SRT1720 treatment did not statistically change pSer637-Drp1 expression. These data illuminated that Drp1 expression and activity were up-regulated in spinal cord of BCP rats and SIRT1 activation reversed Drp1 expression without affect its activity.

3.7. SIRT1 activation regulates Drp1 expression in SHSY-5Y cells

To verify the regulation of SIRT1 on Drp1, SHSY-5Y cells were treated with 0, 1, 10 μM SRT1720 for 24 h. There was no obvious toxicity of 0–10 μM SRT1720 on SHSY-5Y cells (Fig. S1). Then total and phosphorylated Drp1 (Ser637) were measured by immunofluorescence staining and western blotting. Immunostaining showed that compared with control group, Drp1 fluorescence signal intensities decreased and pSer637-Drp1-fluorescene signal intensities relevantly increased in SRT1720-treated group ($P < 0.05$, Fig. 7A and B). Moreover, western blot analysis showed that Drp1 protein level was down-regulated in a SRT1720 dose-dependent manner (Fig. 7D). The levels of Drp1 protein were reduced to 79 ± 6% ($P < 0.05$) and 51 ± 3% ($P < 0.05$) after treatment with 1 and 10 μM SRT1720 (Fig. 7F). The level of pSer637-Drp1 was also down-regulated by SRT1720 (10 μM) treatment. However, there is no statistical difference of Drp1 activity (represented by pDrp1/Drp1) between SRT1720 treated and untreated cells. These data indicated that SRT1720 decreased Drp1 expression in SHSY-5Y cells.

3.8. SRT1720 inhibits CCCP-induced mitochondrial membrane potential decrease in SH-SY5Y cells

Drp1-dependent mitochondrial fission changes mitochondrial membrane potential (MMP) and is closely associated with apoptosis [36]. Fluorescent probe JC-1 was used specific for measuring and analyzing MMP changes, which selectively enter into mitochondria and spontaneously formed complex known as JC-1 aggregates with red fluorescence. When MMP was lost, JC-1 dissipated into monomers (green) and promoted cells became apoptosis [37]. Therefore, JC-1 assay was used to detect the effect of SRT1720 on MMP and apoptosis

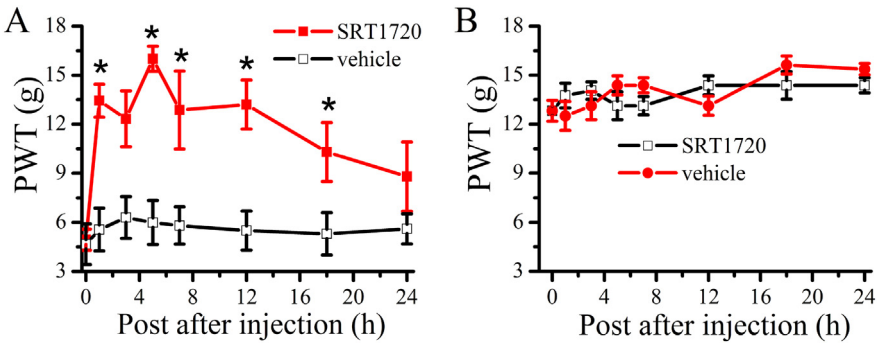

Fig. 4. SRT1720 treatment reversed PWT in BCP rats. A. PWT of BCP rats on POD 12 after intrathecal injection of vehicle and SRT1720. (black □: vehicle treated BCP rats, red ●: 0.5 mg/kg SRT1720 treated BCP rats). B. PWT of normal rats after intrathecal injection of vehicle and SRT1720. (black □: vehicle treated BCP rats, red ●: 0.5 mg/kg SRT1720 treated BCP rats). All data were expressed as the mean ± SEM, n = 9. $^{*}P < 0.05$ vs. BCP rats at each corresponding time point.

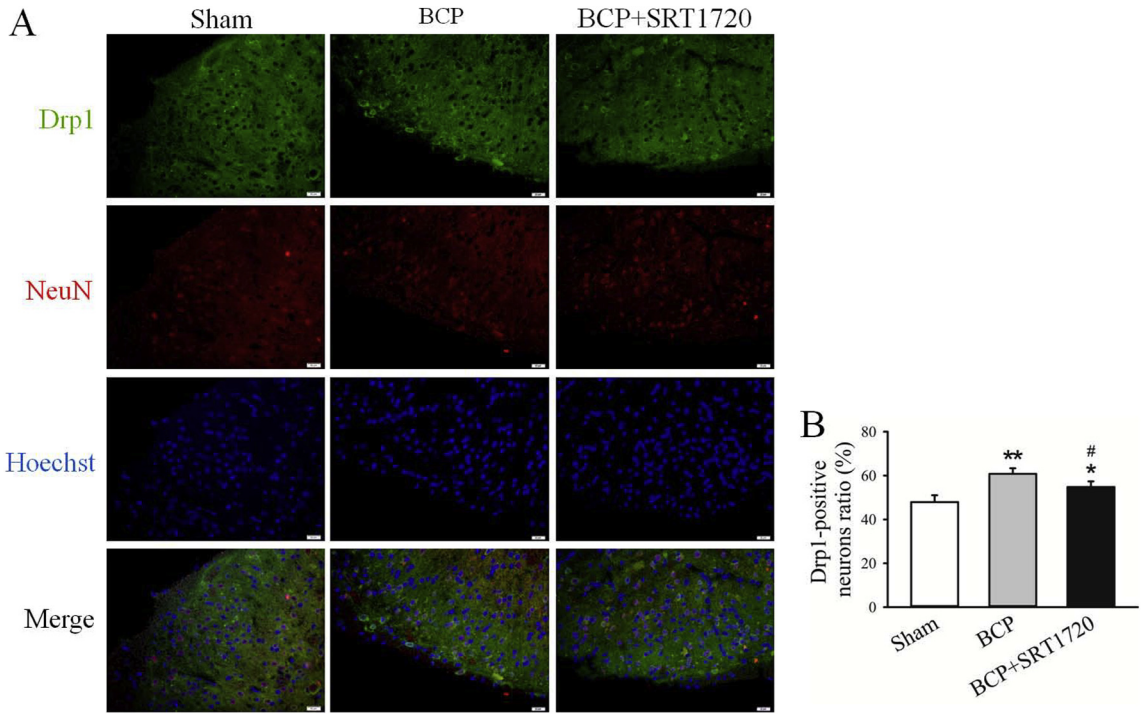

Fig. 5. SRT1720 treatment decreases Drp1-positive neurons in spinal cord of BCP rats. A. Immunofluorescence staining was used to analyze Drp1-positive neurons in spinal cord of sham rats (first lane), BCP rats (second lane) and BCP + SRT1720 rats (third lane). Spinal cord was stained with anti-NeuN antibody (red), and anti-Drp1 antibody (green). Co-localization of Drp1 and NeuN was shown in merged images (yellow). Tissue slices were counterstained with hoechst 33342 (blue). Scale bar = 100 μm. Data present were representative of three independent experiments. B. The ratio of Drp1-positive neurons in spinal dorsal horn was shown in different groups. Data were analyzed using one-way analysis of variance (ANOVA) with post hoc protected least significant difference (PLSD) test. $^{*}P < 0.05$, $^{**}P < 0.01$ vs. sham group; $^{\#}P < 0.05$ vs. BCP group, mean ± SD, n = 5–6 rats.

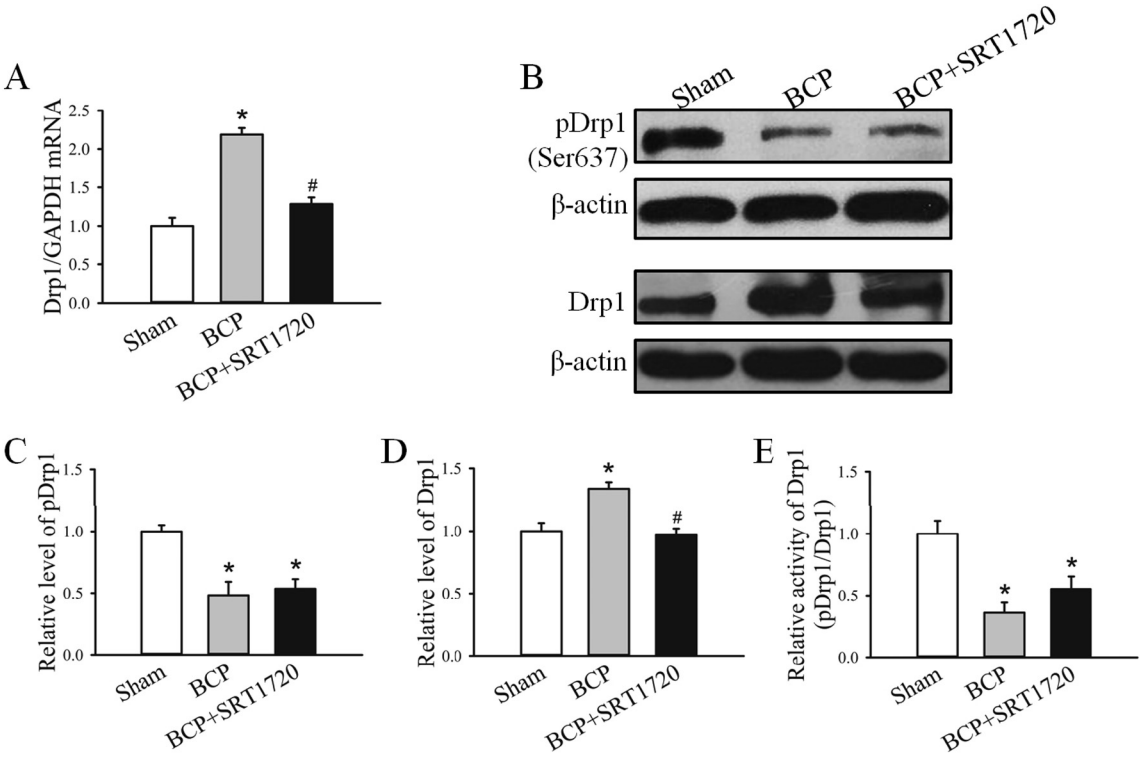

Fig. 6. Effects of SRT1720 on Drp1 expression in BCP rats. A. Total spinal cord RNA was extracted, and Drp1 mRNA level was determined by qRT-PCR analysis. Relative gene expression level was normalized to GAPDH mRNA and expressed as fold change. B. Western blot analysis of protein extracts from sham, BCP and BCP + SRT1720 showing the levels of Drp1 and pSer637-Drp1 protein. C-E. Quantitative analysis of total and phosphorylated Drp1 protein level was shown as the mean ± SD from three independent experiments. $^{*}P < 0.05$ vs. sham group, $^{\#}P < 0.05$ vs. BCP group.

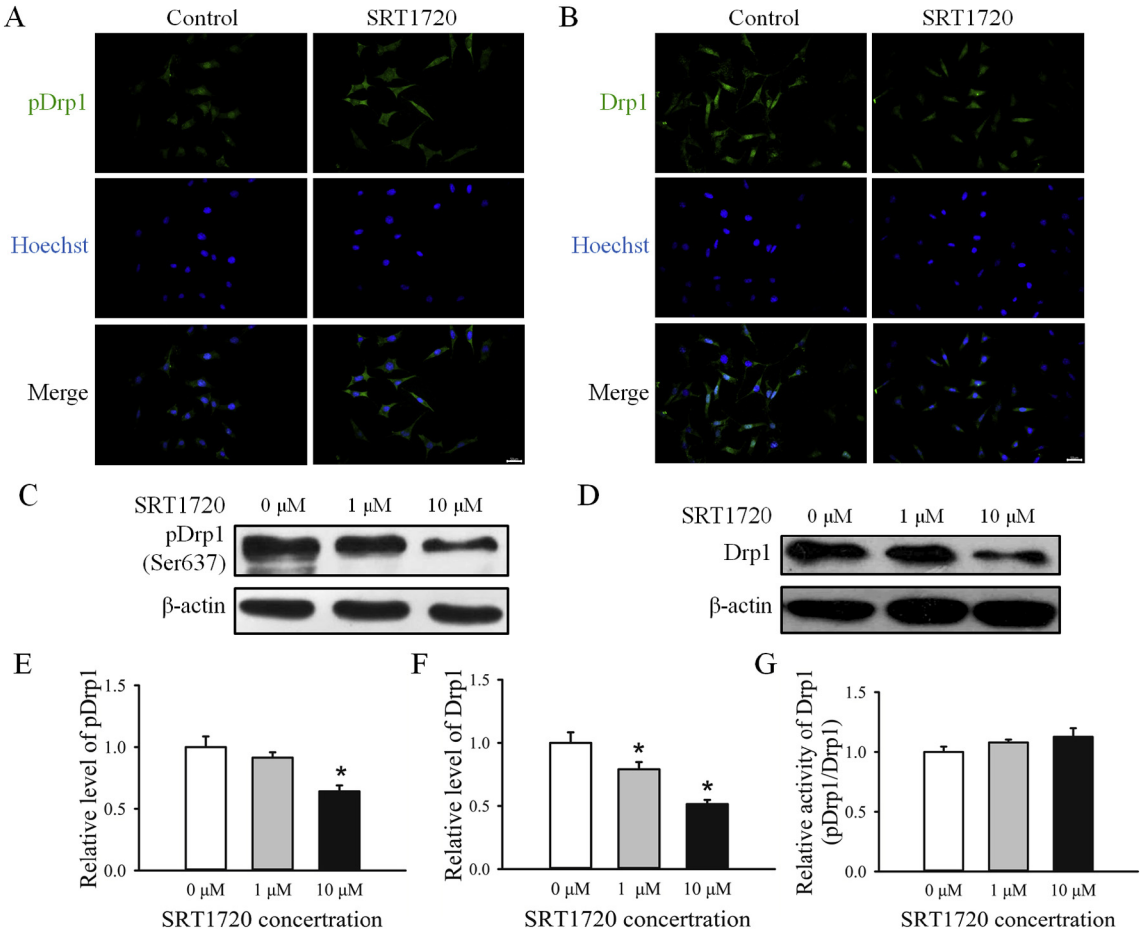

Fig. 7. Effects of SRT1720 treatment on Drp1 expression in SHSY-5Y cells. A-B. After SRT1720 treatment, SHSY-5Y cells were fixed and subjected to immunofluorescence. Anti-Drp1 antibody and anti-pDrp1 were probed with anti-rabbit IgG H&L (FITC) (green) and cells were counterstained with hoechst 33342 (blue). Scale bar = 50 μM. C-D. Western blot analysis of Drp1 protein level in SHSY-5Y cells treated with 0, 1 and 10 μM SRT1720 for 24 h. E-G. Quantification of relative levels of Drp1 and pDrp1 in SRT1720 treated and control cells. Results were shown as the mean ± SD from three independent experiments. *$P < 0.05$. *$P < 0.05$ vs. control group.

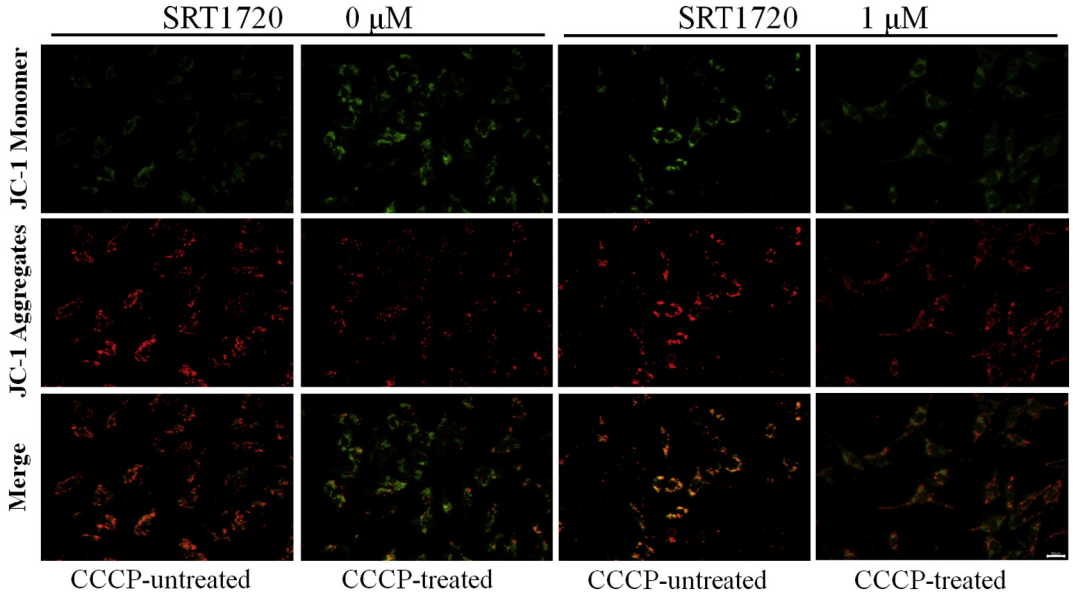

Fig. 8. Effect of SRT1720 on MMP changes. Representative fluorescent images of JC-1 in control and SRT1720 treated SH-SY5Y cells. CCCP was used as a positive control. Green fluorescence on first line represented monomeric JC-1; red fluorescence on second line represented aggregate JC-1. Scale bar = 50 μm.

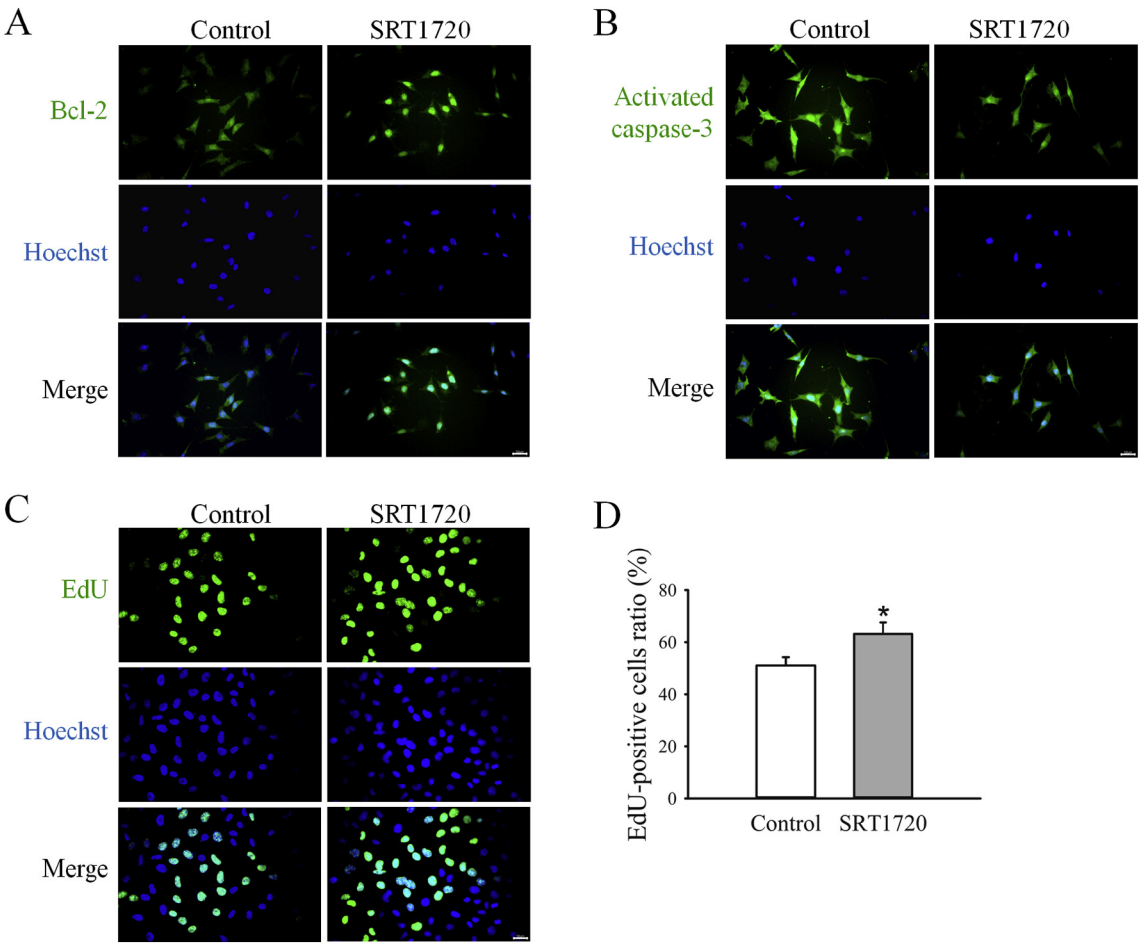

Fig. 9. Changes of apoptosis and proliferation in SH-SY5Y cells upon SRT1720 treatment. A-B. Anti-Bcl-2 and anti-activated-caspase-3 antibodies were probed with anti-rabbit IgG H&L (FITC) (green). Cells were counterstained with hoechst 33342 (blue). Scale bar = 50 μm. C. SRT1720 (0 and 1 μM) was used to treat cells for 24 h. DNA synthesis was measured by EdU assay. D. Quantitative analysis of the percentage of EdU positive nuclei expressed as percentage of the total nuclei number. *$P < 0.05$ compared with control group.

in vitro. As shown in Fig. 8, SH-SY5Y cells were treated with 0 and 1 μM SRT1720 exhibited red fluorescence, confirming high MMP. As a positive control, SH-SY5Y cells were exposed to CCCP, and exhibited green fluorescence with little red fluorescence, indicating low MPP. When cells were treated with SRT1720 for 24 h and combined with exposure to CCCP, JC-1 still showed red fluorescence, indicating SRT1720 inhibited CCCP-induced decrease of MMP. These data demonstrated that SRT1720 increased MMP and inhibited mitochondrial apoptosis.

3.9. SRT1720 reduces apoptosis and promotes proliferation in SH-SY5Y cells

Effects of SRT1720 on cell apoptosis and proliferation were detected using immunofluorescence staining and EdU assay. In SRT1720 treated group, anti-apoptotic factor Bcl-2 fluorescent signal intensities increased (Fig. 9A), and on the contrary, activated-caspase-3 fluorescent signal intensities decreased (Fig. 9B). EdU assay was used to investigate whether SRT1720 promoted cell proliferation. Results showed that SRT1720 dramatically promoted DNA synthesis in SH-SY5Y cells (Fig. 9C and D). Percentages of EdU positive neurons in control group and SRT1720 treated group were 51.2 ± 3.2% and 63.1 ± 4.4%, respectively, which suggested EdU-positive cells were increased by SRT1720 treatment ($P < 0.05$).

3.10. PGC-1α is involved in SRT1720-mediated anti-nociceptive effect on BCP rats

It was reported that mitochondrial biogenesis was promoted by peroxisome proliferator-activated receptor gamma and coactivator 1 alpha (PGC-1α) activation which is mediated by SIRT1-induced deacetylation [38]. Then, PGC-1α expression was detected in rats and cells. As shown in Fig. 10, BCP decreased PGC-1α expression in spinal cord of rats ($P < 0.05$ vs. sham group). SRT1720 treatment increased PGC-1α level in SH-SY5Y cells ($P < 0.05$) measured by western blotting and immunofluorescence staining. And in isolated mitochondria, PGC-1α protein level was up-regulated ($P < 0.05$ vs. control group). The results indicated that PGC-1α was involved in SRT1720-mediated anti-nociceptive effect on BCP rats.

4. Discussion

4.1. SIRT1 dysfunction could be a critical cause of BCP

Neurochemical changes and cellular reorganization in spinal cord are induced by bone cancer pain including profound astrocytosis and pro-inflammatory cytokines releasing [39]. In this study, we found spinal cord of BCP rats exhibited more inflammatory cells infiltration and apoptosis, and down-regulated SIRT1 expression and activity, which is well known as a regulator of DNA damage and cell death/survival [40]. Agonist of SIRT1, SRT1720 treatment activated SIRT1,

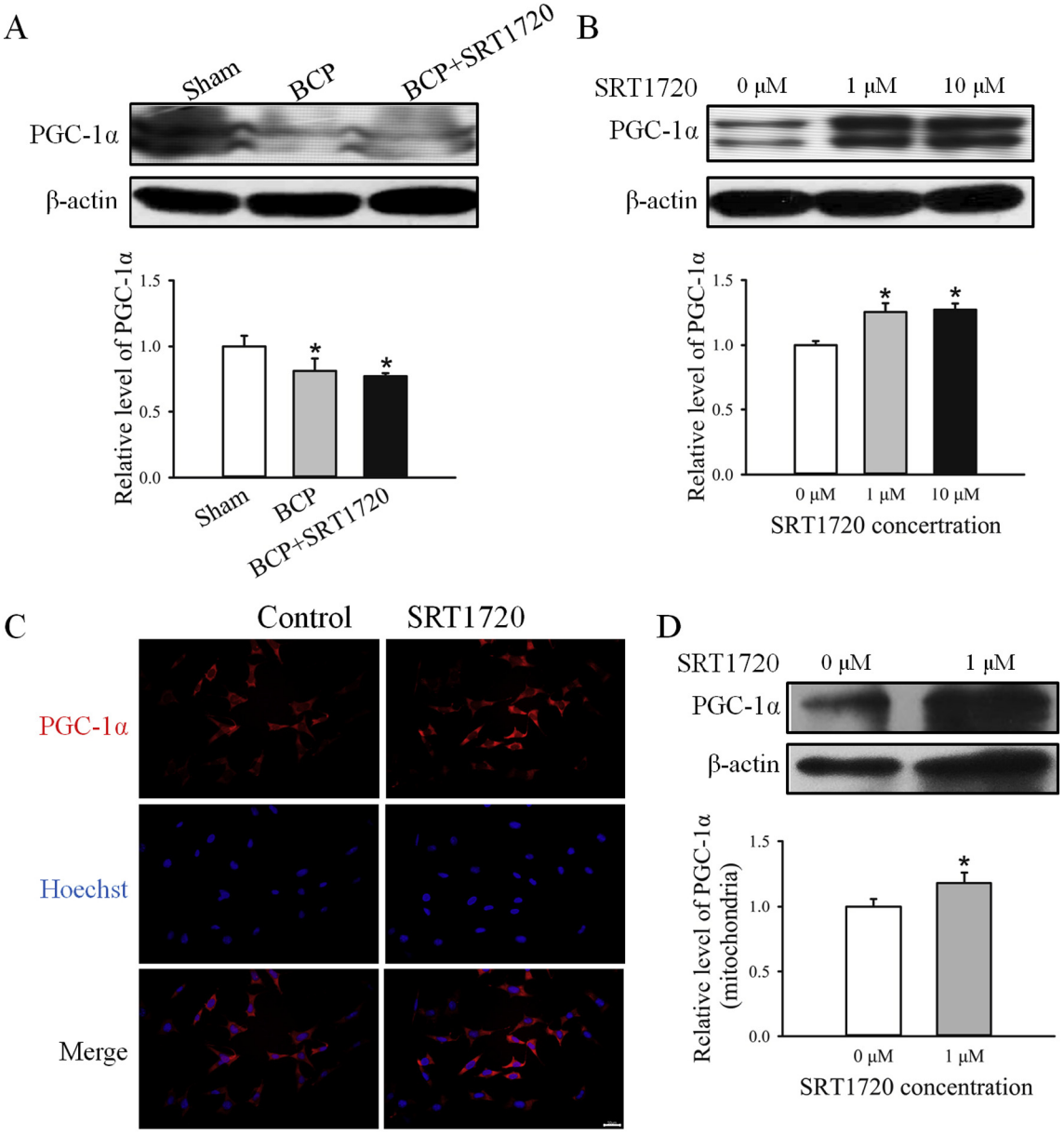

Fig. 10. Effect of SRT1720 on PGC-1α level. A. Western blot analysis of PGC-1α protein levels in spinal cord of BCP rats. Results were shown as the mean ± SD from three independent experiments. *$P < 0.05$ vs. sham group. B. Western blot analysis of PGC-1α protein level in SHSY-5Y cell treated with 0, 1 and 10 μM SRT1720 for 24 h. Results were shown as the mean ± SD from three independent experiments. *$P < 0.05$ vs. control group. C. Anti-PGC-1α antibody was probed with anti-rabbit IgG (FITC) (green). Cells were counterstained with hoechst 33342 (blue). Scale bar = 50 μm. D. Western blot analysis of PGC-1α protein level in isolated mitochondria. Results were shown as the mean ± SD from three independent experiments. *$P < 0.05$ vs. control group.

reversed pain behavior of BCP rats and had a significantly anti-nociceptive effect in BCP. Our previous study reported that SIRT1 expression was down-regulated in DRG neurons of BCP rats, resveratrol (non-specific agonist of SIRT1) treatment activated AMPK-SIRT1-autophagy signal, subsequently reversed pain behavior [13]. Accordingly, abnormal regulation of SIRT1 was closely related to pathology and maintenance of BCP, and may be a potential target for BCP therapy.

4.2. SIRT1 regulates mitochondrial fission via activating PGC-1α

A large number of evidences suggest that PGC-1α was activated by deacetylation through SIRT1 activation, and subsequently promoted mitochondrial gene transcription and mitochondrial biogenesis [41]. SIRT1-mediated deacetylation and activation of PGC-1α becomes an important response of cell to increase mitochondria metabolism when energy is needed. In diabetes-induced cardiac dysfunction model, increases SIRT1 and PGC-1α expression reduces Drp1-mediated mitochondrial fission [42]. In kidney ischemia-reperfusion injury model, activation of SIRT1/PGC-1α pathway recovers mitochondrial protein expression and function to the normal level [43]. In BCP animal model, we found PGC-1α was down-regulated in spinal cord (Fig. 7A and B), and in vitro experiment proved that SRT1720 had an effect on promoting PGC-1α expression in cell lysates and isolated mitochondria. However, in spinal cord of BCP rats, SRT1720 treatment didn't induce increase in PGC-1α expression (Fig. 10). We presumed that the post-translational modifications (PTMs) contributed the difference. PGC-1α activity was modulated through its expression and PTMs, such as phosphorylation, acetylation and ubiquitination. PTMs of PGC-1α constituted the first, fast response to acute stimulus, whereas, the amounts modulation represented a slower adaptive response to more prolonged signal [38]. Therefore, we supposed that in BCP rats, SIRT1 activation by SRT1720 promoted PGC-1α deacetylation and activity. In

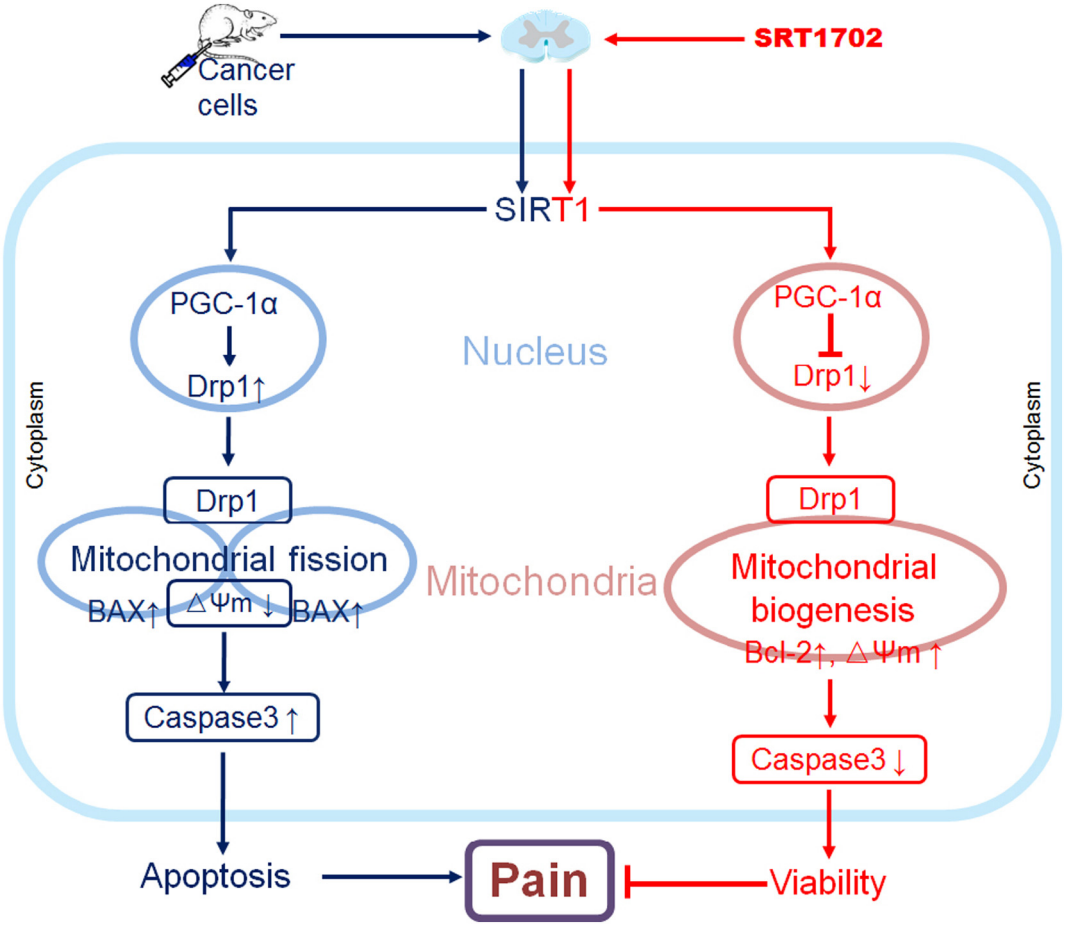

Fig. 11. Schematic representation of SIRT1 modulation of Drp1-mediated mitochondrial fission.
A working hypothesis showing that activation of SIRT1 ameliorates bone cancer pain. SRT1720 activated SIRT1 and inhibited Drp1 expression. As a consequence, effect of Drp1 on mitochondrial fission is attenuated, which increases cell viability and pain behavior is reversed in BCP rats. ΔΨm presents mitochondrial membrane potential changes.

SH-SY5Y cells, SRT1720 increased PGC-1α activity by amounts modulation.

SIRT1/PGC-1α pathway modulates Drp1 expression and mitochondrial fission. Overexpression of PGC-1α reduces Drp1 expression and promotes Drp1-mediated mitochondrial biogenesis. Mutation of PGC-1α reduces mitochondrial function and oxidative capacity [43]. PGC-1α regulates Drp1 via direct action and indirect action. The former is that PGC-1α binds Drp1 promoter [44] and the latter is that PGC-1α decreases Drp1-mediated mitochondrial fission by inhibiting PINK/Parkin expression [45]. We found SRT1720 treatment increased PGC-1α levels in isolated mitochondria (Fig. 10D). Accordingly, PGC-1α was involved in SRT1720 regulated mitochondrial fission in BCP rats.

4.3. SRT1720 inhibits mitochondrial dysfunction induced cell apoptosis in BCP rats

Up-regulation of Drp1 caused mitochondrial fragment and MMP reduction, which was an initial and irreversible step towards apoptosis [46]. In spinal cord of BCP rats, expression of mitochondrial fission related protein Drp1 increased. SRT1720 treatment reduced Drp1 expression to normal level in BCP rats, and decreased Drp1 expression in a SRT1720 dose-dependent manner in SH-SY5Y cells. Moreover, SRT1720 treatment inhibited CCCP-induced MMP reduction, indicating SRT1720 inhibited Drp1-mediated apoptosis.

Bcl-2 family members were involved in mitochondrial dynamics during apoptosis. Bcl-2 was an inner mitochondrial membrane protein, stabled mitochondrial complexes, prevented BAX activation and cell death [47]. BAX was inserted in mitochondrial outer membrane, increased permeabilization of mitochondrial outer membrane, triggered cytochorome c release, activated caspases and promoted intrinsic apoptosis [48]. We found increased BAX, decreased Bcl-2 and activated caspase-3 in spinal cord of BCP while SRT1720 treatment reversed these factors to the normal (sham) level. Similar effects of SRT1720 on these proteins expression in SHSY-5Y cells were also observed and it promoted cell proliferation. Taken together, these data indicated that SIRT1 activation had inhibitory effect on mitochondrial fission induced cell apoptosis.

In summary, our study demonstrates that pain behavior induced by Drp1-mediated mitochondrial fission is triggering by dysregulation of SIRT1 (Fig. 11). SRT1720 reverses pain behavior by activating SIRT1/PGC-1α/Drp1 pathway and consequence inhibits mitochondrial fission associated apoptosis. The current findings in our research provide SIRT1 as a potential target for treating bone cancer pain.

Supplementary data to this article can be found online at https://doi.org/10.1016/j.bbadis.2018.12.017.

Transparency document

The Transparency document associated with this article can be found, in online version.

Acknowledgements

This study was supported by Research Project of Hubei Provincial

Department of Education (No. Q20172804, B2017177 and B2018174), National Natural Science Foundation of China (No. 81641154) and Research Project of pharmacy key subject (2018-19XYZ04).

References

[1] P. Mantyh, Bone cancer pain: causes, consequences, and therapeutic opportunities, Pain 154 (Suppl. 1) (2013) S54–S62.
[2] P.W. Mantyh, Bone cancer pain: from mechanism to therapy, Curr. Opin. Support. Palliat. Care 8 (2014) 83–90.
[3] M.M. Han, C.W. Yang, C.W. Cheung, J. Li, Blockage of spinal endothelin A receptors attenuates bone cancer pain via regulation of the Akt/ERK signaling pathway in mice, Neuropeptides 68 (2018) 36–42.
[4] R.E. Coleman, Clinical features of metastatic bone disease and risk of skeletal morbidity, Clin. Cancer Res. 12 (2006) 6243s–6249s.
[5] B. Nicholson, Responsible prescribing of opioids for the management of chronic pain, Drugs 63 (2003) 17–32.
[6] C. Dong, R. Wu, J. Wu, J. Guo, F. Wang, Y. Fu, Q. Wang, L. Xu, J. Wang, Evaluation of bone cancer pain induced by different doses of Walker 256 mammary gland carcinoma cells, Pain Physician 19 (2016) E1063–E1077.
[7] R.K. Portenoy, Treatment of cancer pain, Lancet 377 (2011) 2236–2247.
[8] G. Lu, J. Li, H. Zhang, X. Zhao, L.J. Yan, X. Yang, Role and possible mechanisms of Sirt1 in depression, Oxidative Med. Cell. Longev. 2018 (2018) 8596903.
[9] L. Qiu, Y. Luo, X. Chen, Quercetin attenuates mitochondrial dysfunction and biogenesis via upregulated AMPK/SIRT1 signaling pathway in OA rats, Biomed. Pharmacother. 103 (2018) 1585–1591.
[10] L.L. Wang, D.L. Shi, H.Y. Gu, M.Z. Zheng, J. Hu, X.H. Song, Y.L. Shen, Y.Y. Chen, Resveratrol attenuates inflammatory hyperalgesia by inhibiting glial activation in mice spinal cords, Mol. Med. Rep. 13 (2016) 4051–4057.
[11] Y. Gui, J. Zhang, L. Chen, S. Duan, J. Tang, W. Xu, A. Li, Icariin, a flavonoid with anti-cancer effects, alleviated paclitaxel-induced neuropathic pain in a SIRT1-dependent manner, Mol. Pain 14 (2018) (1744806918768970).
[12] H. Shao, Q. Xue, F. Zhang, Y. Luo, H. Zhu, X. Zhang, H. Zhang, W. Ding, B. Yu, Spinal SIRT1 activation attenuates neuropathic pain in mice, PLoS One 9 (2014) e100938.
[13] H. Zhu, J. Ding, J. Wu, T. Liu, J. Liang, Q. Tang, M. Jiao, Resveratrol attenuates bone cancer pain through regulating the expression levels of ASIC3 and activating cell autophagy, Acta Biochim. Biophys. Sin. Shanghai 49 (2017) 1008–1014.
[14] C. Lv, H.Y. Hu, L. Zhao, H. Zheng, X.Z. Luo, J. Zhang, Intrathecal SRT1720, a SIRT1 agonist, exerts anti-hyperalgesic and anti-inflammatory effects on chronic constriction injury-induced neuropathic pain in rats, Int. J. Clin. Exp. Med. 8 (2015) 7152–7159.
[15] C.H. Zhou, M.X. Zhang, S.S. Zhou, H. Li, J. Gao, L. Du, X.X. Yin, SIRT1 attenuates neuropathic pain by epigenetic regulation of mGluR1/5 expressions in type 2 diabetic rats, Pain 158 (2017) 130–139.
[16] I. Amigo, F.M. da Cunha, M.F. Forni, W. Garcia-Neto, P.A. Kakimoto, L.A. Luevano-Martinez, F. Macedo, S.L. Menezes-Filho, J. Peloggia, A.J. Kowaltowski, Mitochondrial form, function and signalling in aging, Biochem. J. 473 (2016) 3421–3449.
[17] R. Kandimalla, P.H. bluedy, Multiple faces of dynamin-related protein 1 and its role in Alzheimer's disease pathogenesis, Biochim. Biophys. Acta 1862 (2016) 814–828.
[18] M. Manczak, R. Kandimalla, X. Yin, P.H. Reddy, Mitochondrial division inhibitor 1 reduces dynamin-related protein 1 and mitochondrial fission activity, Hum. Mol. Genet. (2018), https://doi.org/10.1093/hmg/ddy399.
[19] M. Manczak, P.H. Reddy, Mitochondrial division inhibitor 1 protects against mutant huntingtin-induced abnormal mitochondrial dynamics and neuronal damage in Huntington's disease, Hum. Mol. Genet. 24 (2015) 7308–7325.
[20] M. Williams, M.C. Caino, Mitochondrial dynamics in type 2 diabetes and cancer, Front. Endocrinol. (Lausanne) 9 (2018) 211.
[21] S.L. Archer, Mitochondrial fission and fusion in human diseases, N. Engl. J. Med. 370 (2014) 1074.
[22] M. Manczak, H. Sesaki, Y. Kageyama, P.H. Reddy, Dynamin-related protein 1 heterozygote knockout mice do not have synaptic and mitochondrial deficiencies, Biochim. Biophys. Acta 1822 (2012) 862–874.
[23] H.R. Waterham, J. Koster, C.W. van Roermund, P.A. Mooyer, R.J. Wanders, J.V. Leonard, A lethal defect of mitochondrial and peroxisomal fission, N. Engl. J. Med. 356 (2007) 1736–1741.
[24] H. Kanda, S. Liu, T. Iida, H. Yi, W. Huang, R.C. Levitt, D.A. Lubarsky, K.A. Candiotti, S. Hao, Inhibition of mitochondrial fission protein reduced mechanical allodynia and suppressed spinal mitochondrial superoxide induced by Perineural human immunodeficiency virus gp120 in rats, Anesth. Analg. 122 (2016) 264–272.
[25] L.F. Ferrari, A. Chum, O. Bogen, D.B. Reichling, J.D. Levine, Role of Drp1, a key mitochondrial fission protein, in neuropathic pain, J. Neurosci. 31 (2011) 11404–11410.
[26] K. Nishida, T. Matsushita, K. Takayama, T. Tanaka, N. Miyaji, K. Ibaraki, D. Araki, N. Kanzaki, T. Matsumoto, R. Kuroda, Intraperitoneal injection of the SIRT1 activator SRT1720 attenuates the progression of experimental osteoarthritis in mice, Bone Joint. Res. 7 (2018) 252–262.
[27] X.T. Wang, R. Zheng, Z.W. Suo, Y.N. Liu, Z.Y. Zhang, Z.A. Ma, Y. Xue, M. Xue, X. Yang, X.D. Hu, Activity-dependent dephosphorylation of paxillin contributed to nociceptive plasticity in spinal cord dorsal horn, Pain 157 (2016) 652–665.
[28] M. Halperin-Sheinfeld, A. Gertler, E. Okun, B. Sredni, H.Y. Cohen, The tellurium compound, AS101, increases SIRT1 level and activity and prevents type 2 diabetes, Aging (Albany NY) 4 (2012) 436–447.
[29] R.L. Siegel, K.D. Miller, A. Jemal, Cancer statistics, 2017, CA Cancer J. Clin. 67 (2017) 7–30.
[30] W.J. Dixon, Efficient analysis of experimental observations, Annu. Rev. Pharmacol. Toxicol. 20 (1980) 441–462.
[31] A.J. Todd, Neuronal circuitry for pain processing in the dorsal horn, Nat. Rev. Neurosci. 11 (2010) 823–836.
[32] K. Kyrylkova, S. Kyryachenko, M. Leid, C. Kioussi, Detection of apoptosis by TUNEL assay, Methods Mol. Biol. 887 (2012) 41–47.
[33] L. Wen, Z. Chen, F. Zhang, X. Cui, W. Sun, G.G. Geary, Y. Wang, D.A. Johnson, Y. Zhu, S. Chien, J.Y. Shyy, Ca2+/calmodulin-dependent protein kinase kinase beta phosphorylation of Sirtuin 1 in endothelium is atheroprotective, Proc. Natl. Acad. Sci. U. S. A. 110 (2013) E2420–E2427.
[34] K.H. Flippo, A. Gnanasekaran, G.A. Perkins, A. Ajmal, R.A. Merrill, A.S. Dickey, S.S. Taylor, G.S. McKnight, A.K. Chauhan, Y.M. Usachev, S. Strack, AKAP1 protects from cerebral ischemic stroke by inhibiting Drp1-dependent mitochondrial fission, J. Neurosci. 38 (2018) 8233–8242.
[35] A.J. Roe, X. Qi, Drp1 phosphorylation by MAPK1 causes mitochondrial dysfunction in cell culture model of Huntington's disease, Biochem. Biophys. Res. Commun. (2018) pii: S0006-291X(18)30129-3.
[36] S.T. Smiley, M. Reers, C. Mottola-Hartshorn, M. Lin, A. Chen, T.W. Smith, G.D. Steele Jr., L.B. Chen, Intracellular heterogeneity in mitochondrial membrane potentials revealed by a J-aggregate-forming lipophilic cation JC-1, Proc. Natl. Acad. Sci. U. S. A. 88 (1991) 3671–3675.
[37] C.D. Bortner, J.A. Cidlowski, Caspase independent/dependent regulation of K(+), cell shrinkage, and mitochondrial membrane potential during lymphocyte apoptosis, J. Biol. Chem. 274 (1999) 21953–21962.
[38] C. Handschin, B.M. Spiegelman, PGC-1 coactivators and the regulation of skeletal muscle fiber-type determination, Cell Metab. 13 (2011) 351.
[39] C. Lu, Y. Liu, B. Sun, Y. Sun, B. Hou, Y. Zhang, Z. Ma, X. Gu, Intrathecal injection of JWH-015 attenuates bone cancer pain via time-dependent modification of pro-inflammatory cytokines expression and astrocytes activity in spinal cord, Inflammation 38 (2015) 1880–1890.
[40] F. Yeung, J.E. Hoberg, C.S. Ramsey, M.D. Keller, D.R. Jones, R.A. Frye, M.W. Mayo, Modulation of NF-kappaB-dependent transcription and cell survival by the SIRT1 deacetylase, EMBO J. 23 (2004) 2369–2380.
[41] E.J. Kim, J.H. Kho, M.R. Kang, S.J. Um, Active regulator of SIRT1 cooperates with SIRT1 and facilitates suppression of p53 activity, Mol. Cell 28 (2007) 277–290.
[42] S. Nemoto, M.M. Fergusson, T. Finkel, SIRT1 functionally interacts with the metabolic regulator and transcriptional coactivator PGC-1{alpha}, J. Biol. Chem. 280 (2005) 16456–16460.
[43] M. Ding, N. Feng, D. Tang, J. Feng, Z. Li, M. Jia, Z. Liu, X. Gu, Y. Wang, F. Fu, J. Pei, Melatonin prevents Drp1-mediated mitochondrial fission in diabetic hearts through SIRT1-PGC1alpha pathway, J. Pineal Res. 65 (2018) e12491.
[44] R. Cai, T. Yu, C. Huang, X. Xia, X. Liu, J. Gu, S. Xue, E.T. Yeh, J. Cheng, SUMO-specific protease 1 regulates mitochondrial biogenesis through PGC-1alpha, J. Biol. Chem. 287 (2012) 44464–44470.
[45] K. Peng, J. Xiao, L. Yang, F. Ye, J. Cao, Y. Sai, Mutual antagonism of PINK1/Parkin and PGC-1alpha contributes to maintenance of mitochondrial homeostasis in rotenone-induced neurotoxicity, Neurotox. Res. (2018), https://doi.org/10.1007/s12640-018-9957-4.
[46] D.R. Green, L. Galluzzi, G. Kroemer, Mitochondria and the autophagy-inflammation-cell death axis in organismal aging, Science 333 (2011) 1109–1112.
[47] A. Gross, J.M. McDonnell, S.J. Korsmeyer, BCL-2 family members and the mitochondria in apoptosis, Genes Dev. 13 (1999) 1899–1911.
[48] F. Edlich, S. Banerjee, M. Suzuki, M.M. Cleland, D. Arnoult, C. Wang, A. Neutzner, N. Tjandra, R.J. Youle, Bcl-x(L) retrotranslocates Bax from the mitochondria into the cytosol, Cell 145 (2011) 104–116.